THESIS FOR THE DEGREE OF LICENTIATE OF TECHNOLOGY

Alloy Design and Optimization of Mechanical Properties of High-Entropy Alloys

Saad Sheikh

Department of Materials and Manufacturing Technology
CHALMERS UNIVERSITY OF TECHNOLOGY
Gothenburg, Sweden 2016

i

Alloy Design and Optimization of Mechanical Properties of High-Entropy Alloys

Saad Sheikh

Cover: True tensile stress-strain curve for the as-cast $Hf_{0.5}Nb_{0.5}Ta_{0.5}Ti_{1.5}Zr$ with the inset showing fractured surface after tensile testing (More details in paper II)

Alloy Design and Optimization of Mechanical Properties of High-Entropy Alloys

Saad Sheikh

Department of Materials and Manufacturing Technology

Chalmers University of Technology

Abstract

High-entropy alloys (HEAs) are described as alloys containing multi-principal elements in equal or close to equal atomic percentage. HEAs are considered as potential structural materials for high-temperature applications; where alloy design and optimization of mechanical properties is extremely critical. In this regard, achieving both high strength and high tensile ductility is still a great challenge. Compared to conventional alloys, HEAs have high configurational entropy, which tends to stabilize the solid solution formation, mainly face-centered-cubic (fcc) and/or body-centered-cubic (bcc) solid solutions. Generally, fcc-type HEAs are ductile but soft, while bcc-type HEAs are hard but brittle.

One part of this work is to understand the solid solubility in HEAs. The need for single-phase solid solution and controlling the formation of TCP/GCP phases, is addressed through the molecular orbital approach. The output of this approach is the Md parameter, the d-orbital energy level, which can well describe the solubility limit in fcc HEAs comprising of only 3d transition metals. However, Md alone cannot describe the solid solubilities in fcc HEAs, which also contain 4d elements. Alloying of 4d elements with 3d elements will cause a large increase of bond order, Bo, which is the measure of the strength of covalent bonds. The use of two-parameter Md - Bo plot can improve the prediction of solid solubility limit when 4d elements are alloyed, but needs further work. The Md approach for bcc HEAs containing 4d elements is also encouraging, but requires more evidence to support this alloy design approach.

The second part of this work is to ductilize HEAs containing group IV (Ti, Zr, Hf), V (V, Nb, Ta) and VI (Cr, Mo, W) refractory elements where inadequate ductility puts a limit on their mechanical performance for structural applications. A strategy is proposed here to design refractory HEAs with yield strength reaching 900 MPa, and importantly with sufficient ductility at room temperature. Ductility is introduced by maintaining the number of total valence electrons low, which can be controlled by adjusting the alloy compositions. These findings will shed light on the design of refractory HEAs with optimal mechanical properties.

Keywords: High-entropy alloys; alloy design; ductility; mechanical properties; refractory high-entropy alloys; valence electron concentration; topologically closed-pack (TCP) and geometrically closed-pack (GCP) phase

Preface

This licentiate thesis is performed at the Department of Materials and Manufacturing technology at Chalmers University of Technology during the period November 2013-August 2016. This work is funded by Area of Advance (AoA), Materials Science at Chalmers University of Technology, and is carried out under the supervision of Associate Professor Sheng Guo.

List of Appended Papers

Paper I: Saad Sheikh, Uta Klement, and Sheng Guo. Predicting the Solid Solubility Limit in High-Entropy Alloys Using the Molecular Orbital Approach. J. Appl. Phys. **118**, 194902 (2015)

Paper II: Saad Sheikh, Samrand Shafeie, Qiang Hu, Johan Ahlström, Christer Persson, Jaroslav Veselý, Jiří Zýka, Uta Klement, Sheng Guo. Alloy Design for Intrinsically Ductile Refractory High-Entropy Alloys**.**

In Press, J. Appl. Phys., (2016)

Table of contents

1 Introduction

There is a constant need for materials development in structural applications requiring a combination of mechanical properties such as strength, ductility, thermal stability and toughness. Aluminum alloys, iron alloys, titanium alloys, and nickel-based superalloys are some of the major commercially used alloys. Materials which can operate at ever-increasing temperatures have implications on the efficiency of aerospace and power-generation gas-turbines. Turbine blades made of nickel-based superalloys can function at temperatures up to 1200 °C, which is the highest operating temperature. Hottest areas of a turbine engine can even reach 1500 °C, but then thermal barrier coatings and complex cooling systems are incorporated with superalloys. This leads to efficiency losses as large amount of power produced is needed to keep turbine blades cool. A viable solution to reduce such losses is to introduce new ultrahigh temperature structural materials. Perepezko et al. have nicely summarized the development trend for high temperature materials in gas-turbine engines [1]. The correlation based upon the power produced as a function of the turbine rotor inlet temperature is shown in Figure 1.
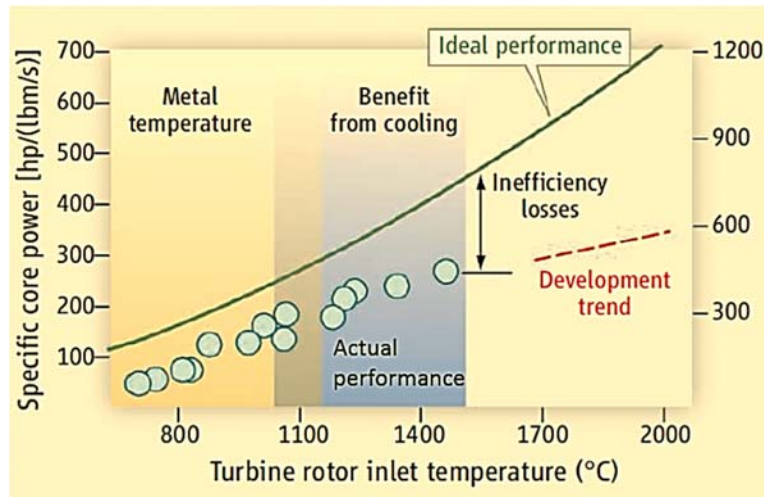

Figure 1: Specific core power versus turbine rotor inlet temperature [1], published with permission from AAAS.

Alternative materials available for high temperature applications are also restricted due to several performance criteria. One of the reported guideline is the Johnson relation, which suggests that if

turbine blades are not protected by coatings and kept uncooled, the melting temperature of the material should be above 2500°C [2]. Higher creep resistance is also desired as blades are subjected to constant stresses from centrifugal force during operation. Only a very few number of intermetallic compounds, ceramics and refractory metals are known that keep the requirement of higher melting temperature. Intermetallic compounds and ceramics also possess good oxidation resistance, but they fail catastrophically due to embrittlement issues and are prone to failure, hence limiting their usage. On the other hand, alloys containing refractory metals, such as molybdenum and niobium alloys fulfill many of the requirements for high temperature applications, but their poor oxidation resistance is also a great challenge that needs to be addressed [3]. There are also issue related to ductility in refractory alloys.

Recently, HEAs have gained significant attention due to their strength, softening resistance, hardness, wear and corrosion resistance, etc [4-6]. They normally form face-centered cubic (fcc) and body-centered cubic (bcc) crystal structure, and sometimes hexagonal close-packed (hcp) structure. The fcc-type HEAs are usually soft and malleable [7]. The bcc-type HEAs has high strength and are usually brittle. Senkov et al. [8-13] has reported a series of bcc refractory HEAs (RHEAs), with high compressive yield strength and hardness, but most of these alloys show low compressive strain at room temperature. On the contrary, tensile properties are more important for engineering and structural application rather than compressive properties. Hence, optimizing strength and tensile ductility in RHEAs is still a challenge.

1.1 Aim of thesis

The two main objectives of this thesis are as follows:

1) Predicting the solid solubility limit in HEAs for alloy design

2) Tuning the ductility for refractory high-entropy alloys (RHEAs)

2   High-entropy alloys

2.1 Introduction of high-entropy alloys

High-entropy alloys (HEAs), proposed by Yeh et al. in 1995 is a rather novel alloy concept, which contain at least five principal elements with the atomic percentage of each element is between 5 % and 35 % [14, 15]. HEAs are an interesting research topic because of their potential in structural and particularly high-temperature structural applications. Depending on the alloy compositions, HEAs tend to form simple solid solution phases, such as fcc and bcc phases. From thermodynamics, it is known that a system tries to minimize its Gibbs free energy (ΔG_{mix}) to achieve a stable or metastable equilibrium state. Enthalpy of mixing (ΔH_{mix}) and total mixing entropy (ΔS_{mix}) are related to Gibbs free energy at a given temperature (T), which is expressed in Kelvin shown by Equation 1[16].

$$\Delta G_{mix} = \Delta H_{mix} - T\Delta S_{mix} \quad (1)$$

Decreasing enthalpy of mixing or increasing mixing entropy can decrease the Gibbs free energy. ΔS_{mix} has four major contributions such as configurational, vibrational, magnetic dipole, and electronic randomness. Among HEAs, the configurational entropy is much higher than in conventional alloys, which usually have one or at most two principal elements [17]. The competition between ΔH_{mix} and $T\Delta S_{mix}$ determines the phase selection if the strain energy effect due to the atomic size difference is not considered. In a high temperature environment, the $T\Delta S_{mix}$ term becomes a dominant factor and is regarded as the main reason behind the formation of simple multi-element solid solutions among HEAs.

From statistical thermodynamics, Boltzmann's equation calculates the configurational entropy of a system [18]. Ideal configurational entropy per mole for a random solid solution with N-components, in which the i*th* component has a mole fraction c_i, is defined as in Equation 2. Entropy would reach a maximum when the alloy is in the equiatomic ratio, and is expressed in Equation 3. R is the gas constant of 8.314 J/ (Kmol).

$$\Delta S_{mix} = -R \sum_{i=1}^{N} c_i \ln c_i \qquad (2)$$

$$\Delta S_{mix} = R \ln N \qquad (3)$$

The configurational entropy increases as the number of elements increases. Table 1 lists the configurational entropies of equiatomic alloys in relation to the gas constant R using Equation 3.

Table 1: Configurational entropies in terms of R with constituent elements up to 13 for equiatomic alloys [19].

n	1	2	3	4	5	6	7	8	9	10	11	12	13
$\Delta S_{mix}/R$	0	0.69	1.1	1.39	1.61	1.79	1.95	2.08	2.2	2.3	2.4	2.49	2.57

Further increasing the number of elements give a limited contribution to the mixing entropy. Configurational entropy of a five element alloy in an ideal case is 1.61 R. High mixing entropy effectively reduces the number of phases and increases mutual solubility among constituent elements.

2.2 Key properties of HEAs

Current knowledge of physical metallurgy is based upon the outcome from conventional alloys, but HEAs are quite different compositionally compared to conventional alloys. Hence, previously established physical metallurgy principles might require modifications regarding HEAs. It is claimed that there are four important features which affect the properties and microstructure of HEAs. These are termed as the high-entropy effect, lattice distortion effect, sluggish diffusion effect and cocktail effect, respectively [14]. Figure 2 shows the schematic of physical metallurgy for HEAs and how it can be utilized to develop, control and utilize materials under the influence of four core effects in HEAs. High-entropy effect should be considered via thermodynamics to determine the equilibrium structure and microstructure. Lattice distortion is related to deformation theory, kinetics and thermodynamics. Sluggish diffusion affects kinetics in transformation among phases. The cocktail effect is due to the outcome of combined effects from crystal structure, composition and microstructure.
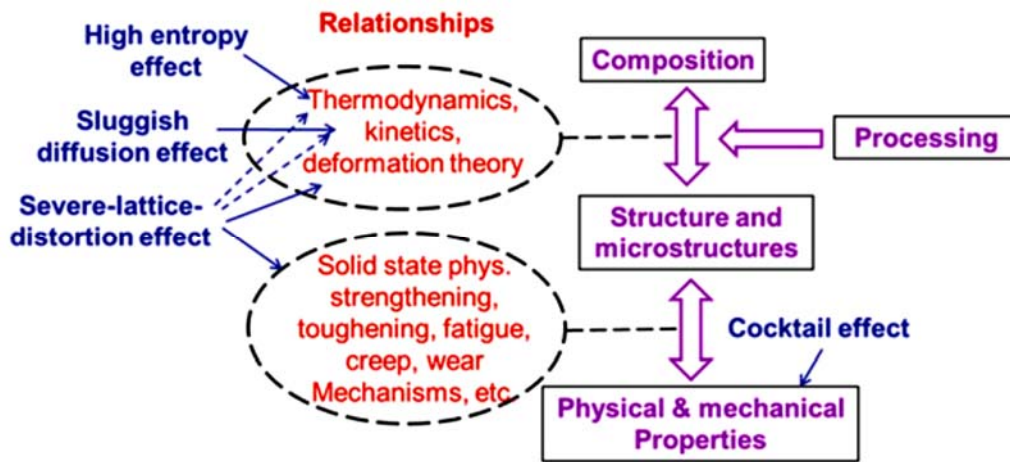
Figure 2: Influenced of four core effects in physical metallurgy of HEAs [20], published with permission from Springer.

High-entropy can enhance solid solution solubility resulting in simpler microstructures. In alloy systems, the high mixing entropy (at high temperatures) competes with mixing enthalpy to lower the Gibbs free energy, thus promoting simple solid solution formation. Solid solution refers to the phase with the complete mixing of all elements in the form of fcc, bcc, and hcp. For the sake of simplicity when defining HEAs, strain energy contribution to enthalpy of mixing from atomic size difference is not considered. One of the widely reported FeCoCrMnNi HEA can form simple fcc solid solution even when annealed [21, 22]. The refractory HfNbTaTiZr alloy forms simple bcc phase in the as-cast state [23].The contribution from higher entropy can limit the formation of intermetallic compounds and elemental phases. Intermetallic compounds have defined stoichiometry and ordered crystal structure. For example, NiAl and Ni_3Ti are of B2 and $D0_{24}$ structure, respectively. Elemental phases are found in the pure component side of a phase diagram. These are terminal solid solution based on one metal element. Figure 3 shows comparisons of the X-ray diffraction (XRD) patterns of an equimolar HEA series of AlCoCrCuFeNiSi in the as-cast condition, starting from binary alloy up to septenary alloy [24]. This HEA series led to only simple fcc and bcc phases, while inhibiting the formation of intermetallic compounds.
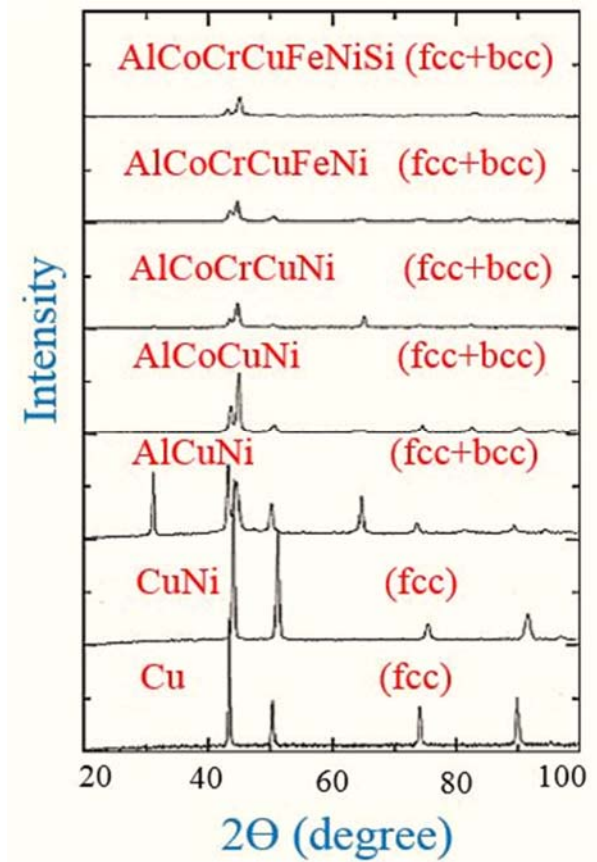
Figure 3: XRD of an equimolar HEA series of AlCoCrCuFeNiSi in the as-cast condition, with alloys containing two up to seven elements [24], published and edited with permission from Elsevier B.V.

Among conventional alloys, most matrix or solvent atoms have the same kind of atoms as their neighbors, resulting in lower lattice distortion in comparison to that of HEAs. Solid solution in HEAs is often a whole solute matrix no matter what crystal structure it acquires. Every atom in the HEAs or multi-principal-element is surrounded by different kinds of atom with different atomic sizes, hence resulting in higher lattice strain. A schematic illustration of a perfect bcc lattice compared to a distorted lattice is shown in Figure 4 [25].
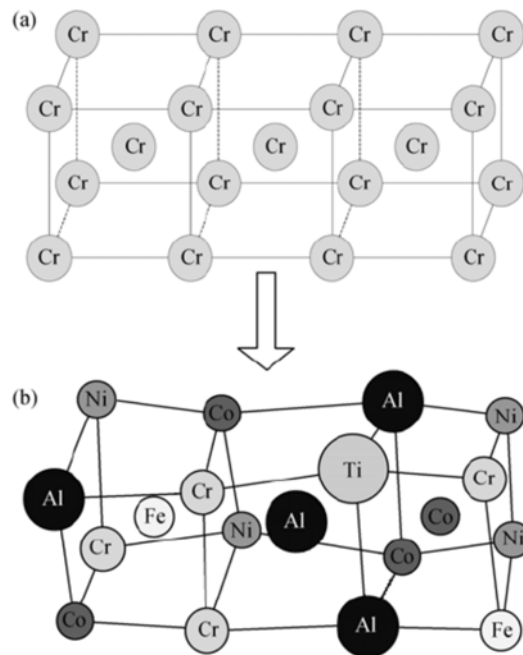
6

Figure 4: Schematic of a bcc structure: (a) an ideal Chromium (Cr) lattice; (b) distorted lattice containing different-sized atoms which are randomly distributed in the crystal lattice [25], published with permission from SP Science in China Press.

Individual crystal structure tendency and bonding energy among constituent elements are also believed to cause higher lattice distortion. Incoherent bindings exist between an atom and its first neighbors, and this incoherency usually varies from site to site in the lattice, resulting in larger severity of lattice [24]. This severity can result in solid solution hardening among HEAs. It is also believed that it might result in lower thermal conductivity compared to that of lower-entropy alloys, which is related to the vibrations of phonons and electrons [26].

Co-operative diffusion of atoms leads to formation of new phases. Among HEAs, each vacancy is affiliated with an excessive entropy of mixing and positive enthalpy of formation, leading to a minimum Gibbs free energy at a given concentration for specific temperature. However, the overall vacancy concentration required for substitutional diffusion is still limited compared to traditional alloys [27]. Diffusional phase transformation might be slower in HEAs vacancy in the solute matrix which is in fact competed and surrounded by different elemental atoms. In short, the sluggish diffusion in HEAs refers to slower phase transformation and diffusion.

In order to verify sluggish diffusion effect through diffusion experiment, single fcc solid solution CoCrFeMnNi was selected for study by Tsai et al. [22]. It was found that diffusion coefficients of each elements at T/T_m in the CoCrFeMnNi HEA system is the lowest, in comparison to dilute CrFeNi(Si) alloys and individual metals such as Co, Fe and Ni, as shown in Figure 5.
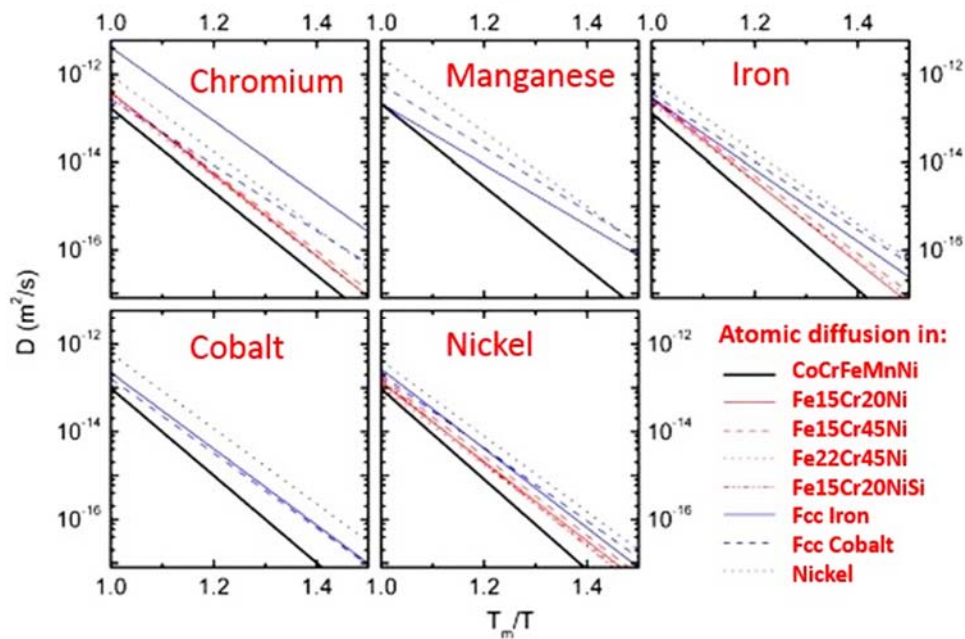

Figure 5: Temperature dependence of diffusion coefficients (D) for elements such Co, Cr, Fe, Mn and Ni in HEAs and conventional alloys [22], published and edited with permission from Elsevier B.V.

HEAs shows rather lower diffusion kinetics compared to the low- or medium-entropy alloys. It is believed that such sluggish diffusion kinetics properties can make them potential candidates for thermal diffusion barrier related applications.

Another characteristic of HEAs, proposed by Ranganathan is ´´multimetallic cocktails´´, which is related to their development and alloy design [28]. A similar effect is also found in conventional alloys, but it is more significant in HEAs due to the contribution to properties from constituent phases, either single phase or multiple phases, depending on the composition and processing route. Hence, this phenomenon, can result in an atomic-scale composite leading to cocktail effects in HEAs.

3   Alloy design and current challenges to HEAs

HEAs are promising for high-temperature applications, due to their compositional flexibility to improve the corrosion and oxidation resistance. Sluggish diffusion and softening resistance at elevated temperatures also gives them advantage for such applications. However, it appears they still have a long way to go in replacing current high-temperature materials. The biggest challenge with HEAs when they are to be utilized in engineering applications is the trade-off between strength and ductility, which is closely related to the choice of suitable constituent elements for desired phase constitution and properties [12, 13]. HEAs form single phase solid solution, but this expression does not hold true for every alloy composition as secondary phase constitutions can occur which includes intermetallic compounds, or even the amorphous phase [29-32].

HEAs with fcc crystal structure are known to be quite ductile, but their strength is low, while bcc HEAs are much stronger and quite often this high strength comes along with brittleness, especially under tension. Alloy design among HEAs, highly relevant to mechanical properties, can be tuned by controlling the valence electron concentration (*VEC*), where addition of elements with higher *VEC* favour the formation of fcc solid solutions, while adding element with lower *VEC* leads to bcc solid solutions [33]. However, the VEC rule is only valid when solid solutions are formed. Despite of the fact that high mixing entropy become effective in stabilizing the formation of solid solutions among HEAs, it is not always the dominant factor as it does not seem to totally eliminate the formation of intermetallic compounds. Apart from high mixing entropy, there are other factors such as mixing enthalpy, atomic size difference, electronegativity that oppose the formation of solid solutions. It still remains a challenge to identify those factors that can eventually result in better phase selection and alloy design. Present alloy design strategies to control the formation of solid solutions, intermetallics and amorphous phases are indeed derived from those which are used for binary solid solutions and metallic glasses. They utilize mostly atomic size mismatch, electronegativity and the mixing enthalpy. In this regard, two-parameter technique, δ - ΔH_{mix} is widely used for alloy design among HEAs [30, 34], where δ is the atomic size mismatch and ΔH_{mix} is the averaged mixing enthalpy of binary equiatomic AB alloys, as defined in Equations 4 and 5.

$$\delta = \sqrt{\sum_{i=1}^{n} c_i \left(1 - r_i / \sum_{j=1}^{n} c_j r_j \right)^2} \qquad (4)$$

$$\Delta H_{mix} = \sum_{i=1, j>i}^{n} 4 \Delta H_{AB}^{mix} c_i c_j, \Delta H_{AB}^{mix} \qquad (5)$$

Where n is the number of alloying elements, c_i and c_j is the atomic percentage for the ith and jth element. r_i or r_i is the atomic radius for the ith or jth element. Solid solutions form when δ is between $1 \leq \delta \leq 6$; and ΔH_{mix} is not notably negative, usually in the range -15 KJ/mol $\leq \Delta H_{mix}$ - 5 KJ/mol. Figure 6 shows the result from the available experimental reported data on the phase selection in HEAs, using the two parameters δ - ΔH_{mix} [34].
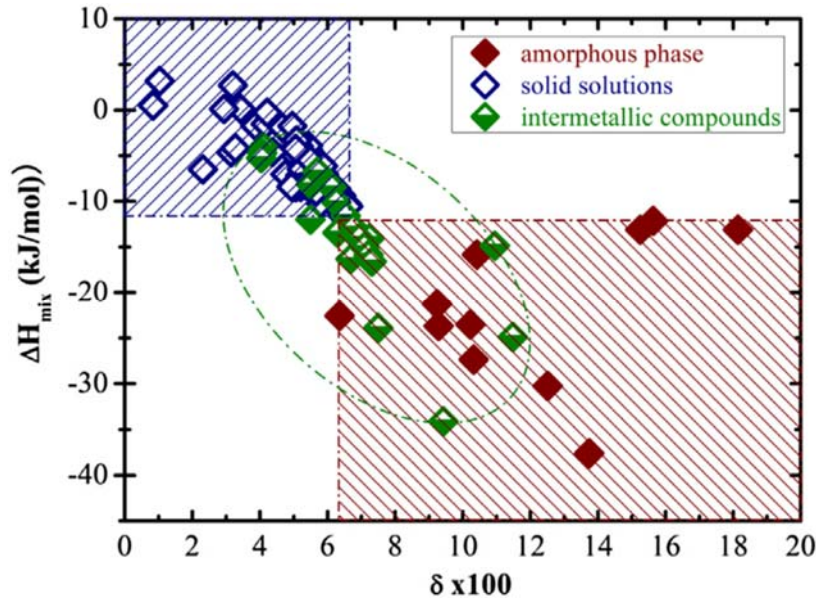

Figure 6: Phase selection in high entropy alloys using δ- ΔH_{mix} with coinciding regions where solid solutions and intermetallics exist as well as amorphous phases and intermetallics [34], published with permission from Elsevier Sci Ltd.

The dotted regions highlight different areas forming solid solutions, intermetallic compounds and the amorphous phase. There exists a coinciding region in the two-dimensional δ- ΔH_{mix} map where both solid solutions and intermetallic exist, and also amorphous phases and intermetallics. This overlap of the curves, i.e. the possibility to form either solid solutions or intermetallic compounds,

is not desirable and prompts to an alternative alloy design criteria, especially when it comes to control the formation of intermetallic compounds from the mechanical properties perspective. Intermetallic compounds have been known to play a critical role in either strengthening or embrittling of alloys. Efforts are usually directed to avoid the formation of intermetallic compounds, particularly topologically closed-pack (TCP) phases and geometrically closed-pack (GCP) phases. TCP and GCP phases can include σ phase, R phase, A15 phase, μ phase, χ phase, and Laves phase/η phase. These are usually undesirable, brittle phases that can form during service. Structurally, TCP phases have close-packed atoms in layers, which are divided by comparatively large interatomic distances, while GCP are close-packed in all directions. The capability to differentiate among the formation of solid solutions and intermetallic compounds, and more specifically, the TCP and GCP phases, is still a challenge to alloy design.

3.1 The *Md* parameter

With the need to explore alternative alloy design opportunities, and to separate the formation of solid solutions and intermetallic compounds, we have determined the prospect of utilizing parameter *Md*, the average energy level of the d orbitals of the alloying transition metals to HEAs, to predict the phase boundaries between solid solutions and TCP/GCP phases [35]. *Md* has been a useful parameter to predict the solid solubility limit in transition-metal-based alloys such as nickel -based, cobalt-based and iron-based alloys. Since HEAs are mostly composed of transition metals, *Md* could also be applicable to HEAs. The parameter *Md,* and its potential to determine solid solubility was introduced by Morinaga et al. [35]. It utilizes cluster calculations to identify the d-orbital energy level of transition element, in a base metal. In the case of a pure Fe cluster, the levels of $8e_g$ to $16t_{2g}$ emerge largely from the Fe 3d orbitals, and establish the Fe 3d band where the Fermi energy level is present [36]. When pure Fe is alloyed, new energy levels mainly due to the d-orbitals of the alloying transition metal emerge above the Fermi energy level. These energy levels varies consistently with the arrangement of elements in the periodic table. The average energy of two such d-orbital levels, e_g and t_{2g}, is *Md*. Some typical *Md* values are listed in Table 2, for various transition metals (M) in fcc Ni, used by Morinaga et al. to determine the solid solubility in nickel base superalloys [37]. Since lattice parameter and crystal structure are similar for Ni and Ni_3Al, the *Md*

11

values for fcc Ni can be used instead. In Table 2, Al and Si are added as non-transition metals, and their *Md* are empirical values and obtained from interpolation [36].

Table 2: List of Md values for common transition metals M in fcc Ni used to determine solid solubility in fcc alloys [37].

	Element M in fcc Ni	*Md* (eV)
3d	Ti	2.271
	V	1.543
	Cr	1.142
	Mn	0.957
	Fe	0.858
	Co	0.777
	Ni	0.717
	Cu	0.615
4d	Zr	2.944
	Nb	2.117
	Mo	1.55
5d	Hf	3.02
	Ta	2.224
	W	1.655
	Re	1.267
others	Al	1.9
	Si	1.9

The average value of *Md* for alloys is defined by taking the compositional average, as given by Equation 6:

$$Md = \sum_{i=1}^{n} c_i (Md)_i \qquad (6)$$

For Ni_3Al, the levels of $13a_{1g}$ to $15e_g$ are predominantly originated from Ni 3d orbitals, i.e., where the Fermi level lies as shown by arrow in figure 7. With the addition of transition elements to Ni_3Al,

new energy levels due to the d orbitals of alloying elements appear above the Fermi level. $16e_g$ and $14t_{2g}$ are shown with dotted levels in Figure 7, and the average energy of two such d-orbital levels correspond to *Md*.
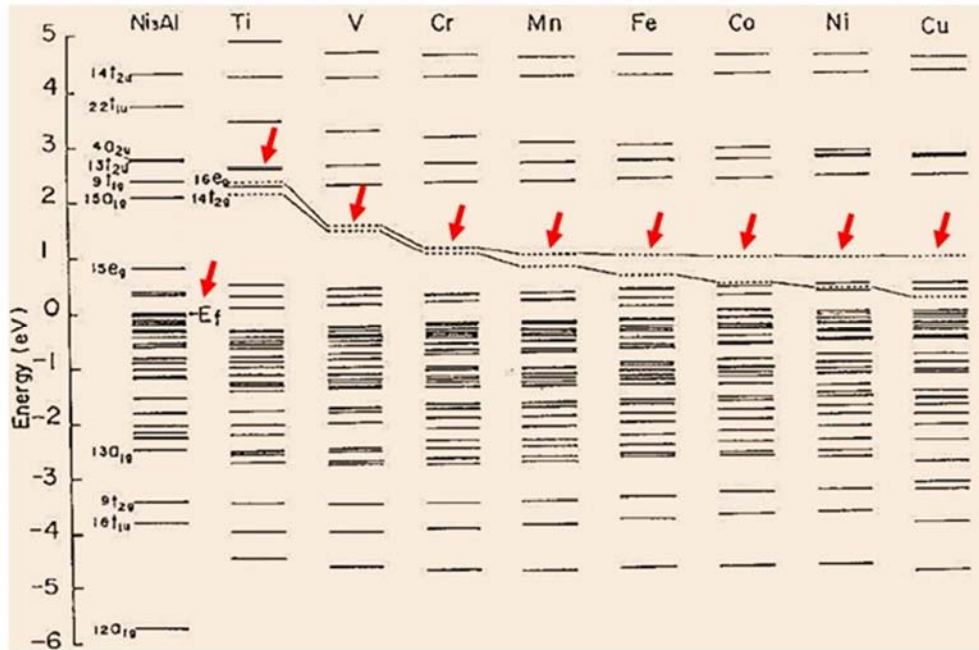

Figure 7: Energy level structures of pure and alloyed Ni₃Al with 3d transition metals [38], published and edited with permission from Springer Science.

The *Md* levels are related to the electronegativity and the atomic radius of elements in a way that as *Md* levels increase, the electronegativity decreases, but increases again with increasing atomic radius of the element [36]. When *Md* increases above a certain limit, the phase instability will occur and secondary phase will appear. A single parameter, the critical *Md* value determines the solubility limit of the terminal solid solution. The critical *Md* value also depends on the type of the secondary phase. To determine the impact of the parameter *Md* on solid solubility among solid solutions and TCP/GCP phases in HEAs, we have inspected a considerable number of HEA systems with reportedly fcc solid solutions and fcc solid solutions plus TCP/GCP phases (σ phase, R phase, μ phase and Laves phase/η phase), as shown in Table 3. The average value of *Md* for alloys is also given.

Table 3: Phase constitutions in fcc structured HEAs containing 3d transition metals, and their d-orbital energy level, Md.

Alloy system	Phase	*Md*	Reference
CoCrCuFeNi	fcc	0.822	[39]
CoCrCu$_{0.5}$FeNi	fcc	0.845	[40]
CoCrFeMnNi	fcc	0.89	[5]
CoCrFeNi	fcc	0.874	[41]
CoCrCuFeNiTi$_{0.5}$	fcc	0.954	[42]
Al$_{0.3}$CoCrCuFeNi	fcc	0.883	[39]
Al$_{0.5}$CoCrCuFeNi	fcc	0.92	[39]
CoCrCuFeMnNi	fcc	0.844	[5]
CoCuFeNiV	fcc	0.902	[30]
Al$_{0.25}$CoCrCu$_{0.75}$FeNi	fcc	0.886	[43]
Al$_{0.5}$CoCrCu$_{0.5}$FeNi	fcc	0.95	[43]
Al$_{0.25}$CoCrFeNi	fcc	0.934	[44]
Al$_{0.375}$CoCrFeNi	fcc	0.961	[44]
Al$_{0.5}$CoCrCuFeNiV$_{0.2}$	fcc	0.942	[45]
CoCrFeNiTi$_{0.3}$	fcc	0.971	[46]
CoCrFeNiSi$_{0.05}$	fcc	0.886	[47]
CoCrFeNiSi$_{0.1}$	fcc	0.899	[47]
CoCrFeNiSi$_{0.15}$	fcc	0.911	[47]
CoCrFeNiSi$_{0.25}$	fcc	0.934	[47]
CoCrFeNiTi$_{0.5}$	fcc+σ+Laves+R	1.029	[46]
CoCrCuFeNiTi$_{0.8}$	fcc+Laves	1.022	[42]
CoCrCuFeNiTi	fcc+Laves	1.063	[42]
Co$_{1.5}$CrFeNi$_{1.5}$Ti$_{0.5}$	fcc+η	0.978	[48]
Al$_{0.3}$CoCrFeNiTi$_{0.1}$	fcc+ η	0.975	[49]

These alloys are all prepared by casting route. We have also included a series of alloys with the composition $CoCrFeNiSi_x$ (where x=0.05, 0.1, 0.15 and 0.25) to determine how well Md can help to predict solid solubility among fcc HEAs. The outcome for Md is mentioned later in the results section and also in the article attached at the end of the thesis.

3.2 Mechanical properties of HEAs

Transition metals are most commonly used to synthesize HEAs. The atomic radii of some of the elements such as Fe, Ni, Cr, Co and Cu are quite similar, and mixing enthalpies among them are rather insignificantly negative. HEAs consisting of such elements have the tendency to form simple fcc solid solutions; as reported by Chen et al., but they are accompanied with low mechanical strength, which is not attractive for applications. Aluminium was added into a CoCrCuFeNi system, and with the increase in Al, the single phase fcc transformed to a combined fcc + bcc solid solution. The hardness values also increased with increasing Al content, which can be related to the increase in lattice distortion and formation of the harder bcc phase [50]. Wang et al. has reported the addition of Al in the $CoCrCuFeNiTi_x$ system with simple fcc solid solution formation, while the amount of Ti was kept lower, but secondary phases started to appear as Ti content was increased [42]. Chen et al. investigated the properties of $Al_{0.5}CoCrCuFeNiTi_x$ by varying Ti content [51]. Simple fcc phase appeared with lower Ti, but as Ti content was increased, a mixture of fcc and bcc phases was formed. By further increasing Ti, Ti_2Ni-like phase (TL) structure and sigma (σ) phases appeared. Having Ti $\geq$ 1.2 atomic ratio, σ phase disappeared, but the mixed fcc, bcc and TL phases were still present. Hardness of the alloy system increased from HV 225 to HV 770 with the increase in the amount of Ti. Change of mechanical strength in this HEA system resulted mainly from the phase transformation from fcc to bcc, and also from the precipitation of inter-metallic compounds, such as σ phase and TL phases. Phase constitution and hardness for $Al_xCoCrCuFeNi$ and $Al_{0.5}CoCrCuFeNiTi_x$ are shown in Table 4:

Table 4: Phase constitution and hardness for Al$_x$CoCrCuFeNi and Al$_{0.5}$CoCrCuFeNiTi$_x$ system with increase in Al content and Ti content respectively [50, 51].

Alloy	Phase constitution	Hardness	Reference
CoCrCuFeNi	fcc	133	[50]
Al$_{0.3}$CoCrCuFeNi	fcc	180	[50]
Al$_{0.5}$CoCrCuFeNi	fcc	208	[50]
Al$_{0.8}$CoCrCuFeNi	fcc+bcc	271	[50]
AlCoCrCuFeNi	fcc+bcc	406	[50]
Al$_{0.5}$CoCrCuFeNiTi$_{0.2}$	fcc	275	[51]
Al$_{0.5}$CoCrCuFeNiTi$_{0.4}$	fcc+bcc	325	[51]
Al$_{0.5}$CoCrCuFeNiTi$_{0.6}$	fcc+bcc	460	[51]
Al$_{0.5}$CoCrCuFeNiTi$_{0.8}$	fcc+bcc+sigma phase	590	[51]
Al$_{0.5}$CoCrCuFeNiTi$_1$	fcc+bcc+sigma phase	630	[51]
Al$_{0.5}$CoCrCuFeNiTi$_{1.2}$	fcc+bcc+sigma phase+TL	650	[51]
Al$_{0.5}$CoCrCuFeNiTi$_{1.4}$	fcc+bcc+TL	660	[51]
Al$_{0.5}$CoCrCuFeNiTi$_{1.6}$	fcc+bcc+TL	670	[51]
Al$_{0.5}$CoCrCuFeNiTi$_{1.8}$	fcc+bcc+TL	680	[51]
Al$_{0.5}$CoCrCuFeNiTi$_2$	fcc+bcc+TL	700	[51]

Ma et al.[52]studied the Nb alloying effect, on AlCoCrFeNb$_x$Ni HEAs system and reported bcc solid solution phase together with ordered Laves phase of (CoCr)Nb-type. The microstructures of the alloy changed from hypoeutectic to hypereutectic, with compressive yield strength and Vickers hardness going through a linear increase with the addition of Nb content, as shown in Table 5.

Table 5: Mechanical properties under compression and Vickers hardness of as-cast AlCoCrFeNbxNi (where x = 0.1, 0.25, and 0.5) alloys [52].

Alloy	$\sigma_{0.2}$ (MPa)	σ_{max} (MPa)	$\varepsilon_{p\ (\%)}$	HV
AlCoCrFeNb$_{0.1}$Ni	1641	3285	17.2	569
AlCoCrFeNb$_{0.25}$Ni	1959	3008	10.5	669
AlCoCrFeNb$_{0.5}$Ni	2473	3170	4.1	747

Results from compression testing shows that the yield strength is substantial increased from 1641 MPa to 2473 MPa, while the plastic strain limit is significantly decreased from 17.2 % to 4.1%, which is due to the Nb addition. It is also found that the plasticity of the alloys is getting progressively worse as a result of the increasing amount of the brittle Laves phase.

3.3 Refractory alloys

The refractory metals have melting points around 2000°C and higher. They consists of the following metals and their alloys: W, Mo, Ta, Nb and Re. Such metals/alloys are used in critical applications where high corrosion resistance and high-temperature strength are required. Even if such metals have high melting points, they need to be alloyed with other elements to be utilized in applications. There is also a wider definition of refractory metals which includes nine other elements such as: Ti, Zr, Hf, V, Cr, Ru, Os, Rh and Ir. These elements also have relatively high melting points. Some of the key properties such as melting point and density are shown in Table 6:

Table 6: Melting point and density of refractory elements [53].

Element	Melting point (° C)	Density (g/cm^3)
Titanium, Ti	1668	4.507
Zirconium, Zr	1855	6.511
Hafnium, Hf	2233	13.31
Vanadium, V	1910	6.11
Niobium, Nb	2477	8.57
Tantalum, Ta	3017	16.65
Chromium, Cr	1907	7.14
Molybdenum, Mo	2623	10.28
Tungsten, W	3422	19.25
Rhenium, Re	3186	21.02
Ruthenium, Ru	2334	12.37
Osmium, Os	3033	22.61
Rhodium, Rh	1964	12.45
Iridium, Ir	2466	22.65

When developing new high-temperature materials systems, factors such as density, melting point and cost are critical. However, two material characteristics influence development strategies significantly, i.e. high temperature creep and oxidation resistance. Usually materials with higher melting temperatures have lower creep rates, hence leading to higher operating temperatures. HEAs naturally possess the advantages to be considered as new types of high-temperature alloys with high softening resistance at elevated temperatures and slow diffusion kinetics. In this regard, refractory high-entropy alloys (RHEAs) based on group IV (Ti, Zr, Hf), V (V, Nb, Ta) and VI (Cr, Mo, W), are attractive for their potential in important high-temperature applications. Unfortunately, they usually lack sufficient ductility at room temperature, which impedes their further development. Senkov et al. studied two RHEAs, $V_{20}Nb_{20}Mo_{20}Ta_{20}W_{20}$ and $Nb_{25}Mo_{25}Ta_{25}W_{25}$, produced by

vacuum arc melting [8, 12]. In the as-cast condition, these alloys have a dendritic microstructure consisting entirely of a single-phase bcc crystal structure. A very high microhardness of Hv = 4.46 GPa and 5.42 GPa is reported for $Nb_{25}Mo_{25}Ta_{25}W_{25}$ and $V_{20}Nb_{20}Mo_{20}Ta_{20}W_{20}$ alloys, respectively. The mechanical behavior of these alloys over a wide temperature range is shown in Figure 8:
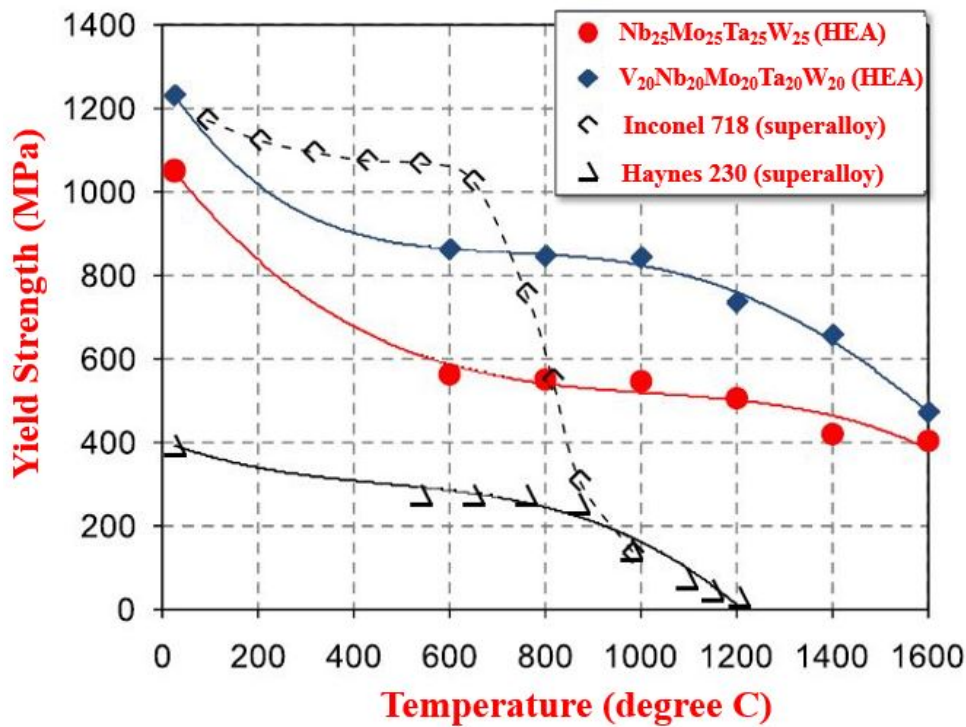

Figure 8: Yield strength variation with temperature of two different RHEAs Nb25Mo25Ta25W25 and V20Nb20Mo20Ta20W20 ; and the two superalloys Haynes 230 [54] and Inconel 718 [55], published and edited with permission from Institute for Scientific Information.

Figure 8 shows the change in yield strength with temperature of two RHEAs as compared to two Ni-based superalloys, Haynes 230 [54] and Inconel 718 [55]. The yield strength of both RHEAs are higher than those of Haynes 230 at all tested temperatures, and it is also higher than those of Inconel 718 at temperatures over 800 °C. Yield strength decreased to 405 MPa for the $Nb_{25}Mo_{25}Ta_{25}W_{25}$ alloy, and for the $V_{20}Nb_{20}Mo_{20}Ta_{20}W_{20}$ to 470 MPa alloy at the maximum reported temperature which is 1600 ° C in this case. The strong resistance to high-temperature softening, in comparison to other alloys, is probably due to sluggish diffusion of elements in the

19

refractory HEAs. It can be also related to high melting points of such alloys. Despite very high temperature strength, there is one big concern for RHEAs, i.e. they lack room temperature ductility. Although they posses high yield strength, both $Nb_{25}Mo_{25}Ta_{25}W_{25}$ *and* $V_{20}Nb_{20}Mo_{20}Ta_{20}W_{20}$ fractured at a mere elongation of 2.6 % and 1.7 % at room temperature, even under compression.

Wu and Zýka have reported the tensile ductility for two RHEAs in equiatomic quaternary HfNbTiZr [56] and equiatomic quinary HfNbTaTiZr [23], but they are unable to give any valid strategy to design ductile RHEAs. It is important to emphasize here on the need to further explore and scrutinize RHEAs to identify the true potential of such materials; especially on the basis of their ductile and brittle behaviour. Continuing with the aim to achieve scientific understanding of the mechanisms controlling ductility, and to propose a guideline to develop rather ductile RHEAs, further advancement is very much desired. Despite knowing that the corrosion and oxidation resistance of alloys at higher temperatures are also important factors in determining their long term stability, here we shall focus on the alloy design, i.e., the development with dual properties of *strength and ductility*.

3.4 Theories for ductility

It is widely recognized that ductility is dependent on material properties and test conditions, which can include grain size, ease of dislocation generation, dislocation density and their mobility, yield strength, surface energy, temperature and strain rate. Given the large number of variables that influence ductility, it is very challenging to improve the inherent ductility. One way to enhance ductility is to control extrinsic features of the alloy (e.g., through grain size modification, secondary particles/precipitate distribution etc.) [57]. This can help limiting the crack propagation and hence postponing material failure. Several theories have been proposed in the past which link basic crystal properties to inherent ductility. Kelly, Tyson, and Cottrell suggested a criterion for ductile and brittle behaviour, stating that a material would be regarded as brittle if the ratio of the largest applied tensile stress to the maximum shear stress close to the crack tip, is greater than the ratio of the theoretical cleavage stress to the theoretical shear strength; otherwise, materials will break with some plastic flow [58]. Rice and Thomson have proposed a parameter expressed as a ratio ($\mu b/\gamma$)

20

to categorize materials according to their brittle or ductile nature. The parameter consists of μ which is the shear modulus of the material, b is the Burgers vector and γ represents the surface energy. Materials for which the ratio ($\mu b/\gamma$) exceeds ~10 would be brittle; materials with a ratio of ($\mu b/\gamma$) less than about ~7.5 would likely behave in a ductile manner [59]. Chan has analyzed the fracture toughness in a quaternary niobium-alloy system by correlating the number of s+d electrons per atoms to the elastic constants [60]. He utilized the ratio of the surface energy to the Peierls–Nabarro barrier energy and the ratio of the surface energy to the unstable stacking fault energy [61, 62]. It has helped in gauging whether dislocation movement/mobility or their emission is more important in determining the effect of alloy concentration on fracture toughness. Chan concluded that dislocation mobility seemed to be a better indicator for the particular alloy system studied [60]. Qi utilized first-principles calculations to study the intrinsic ductility or brittleness of alloys based upon group VI elements such as W and Mo. He proposed that such alloys can become intrinsically ductile if their average valence electron numbers are decreased, which can be controlled by alloying. First-principles calculations show that alloying pure group VI element Mo/W with group IV (Ti, Zr, Hf) or group V transition metals can transform them into intrinsically ductile materials [63]. Li used *ab initio* alloy theory to identify the alloying effect on the ideal tensile strength and elastic properties of RHEAs based on elements such as Ti, Zr, Hf, V and Nb. Their work suggested that intrinsically ductile HEAs can be obtained by controlling the ratio of group IV to group V elements. The effect of alloying ratio on the ideal tensile strength was related to the *d*-band filling [64].

Most of the reported RHEAs show low to medium high compressive plastic strain at room temperature [8, 12], but it is widely accepted that engineering and structural applications require significant mechanical properties in loading under tension rather than under compression. Working on the similar lines to design ductile RHEAs, we have utilized valence electron concentration (*VEC*), which can be important in controlling the mechanical behaviour of refractory metals and to their alloy design. *VEC* has been also quite useful in controlling the hexagonality of Co_3V alloys related to the room temperature ductility where ordered hexagonal alloys are brittle due to the limited number of slip systems *[65]*. *VEC* is defined as the total number of electrons contained in the valence band, including *d*-electrons [66, 67]. It can be determined by the weighted average of each constituent as shown in Equation 7:

$$VEC = \sum_{i}^{n} x_i (VEC)_i \qquad\qquad (7)$$

Where $(VEC)_i$ is the *VEC* for individual element. It is important to note here that *VEC* should not be confused with *e/a* even if both are regarded to be an electron concentration. e/a is the average number of itinerant electrons per atom, which has been widely used in relation to the Hume-Rothery electron concentration rule where identical crystal structures occur at a distinctive e/a. It has also been reported to influence the crystal structure of Hume-Rothery compounds. Despite its importance, one of the major shortcoming in using *e/a* as pointed out by Mizutani is the difficulty in defining the exact *e/a* values for various transition metals [66]. Also *e/a* varies in different environments and can lay uncertainty on its applicability. Compared to e/a, *VEC* seems to be a simpler and direct electron concentration parameter for HEAs. Guo has used *VEC* to delineate the phase stability of fcc or bcc solid solutions among HEAs [29, 33]. He states that at *VEC* < 6.87 bcc solid solution will be formed while fcc phases are found to be stable at higher VEC ($\geq$ 8). However, this knowledge is still insufficient with respect to alloy design for HEAs with optimum mechanical properties, especially for the design of ductile RHEAs.

4 Experimental methods

4.1 Arc melting

The HEAs are prepared in an arc-melting equipment supplied by Edmund Bühler Company. Melting was carried out through vacuum arc-melting a mixture of constituent elements with purity greater than 99.9 wt. % in a Ti-gettered high-purity argon atmosphere. The melting and flipping of samples is repeated at least five times to achieve a good chemical homogeneity of the alloy. It employs a non-consumable tungsten electrode to generate an electric arc that heats up the gas and creates plasma. Rather high vacuum is obtained using both rotary and diffusion pump which can go up to a pressure of 10^{-5} mbar. The casting mold and melting plate on which raw material is placed, are made out of copper in order to conduct heat quickly. The heating chamber and the crucible plate are also water-cooled by an external chiller in order to avoid overheating during the melting process.

4.2 Vickers hardness measurements

Vickers hardness measurement is an indentation technique where the diamond indenter with the geometry of a pyramid is forced onto the surface of a mechanically grinded and polished sample. The diagonals of the indent are measured and Vickers hardness can be determined using Equation 8, where P is load (N) and d (mm) is the mean length of diagonals. In our case, 9.8066 N load is applied for 15 s

$$HV=0.01819 \ P/d^2 \qquad (8)$$

4.3 X-ray diffraction

X-ray diffraction is used for phase identification in materials. The atoms or molecules of the crystal cause a beam of X-rays to diffract into certain directions, producing secondary waves spreading from electrons. Such waves cancel each other in most directions through destructive interference

and constructively in some directions. It can be determined by Bragg's law given in Equation 9, where n is the diffraction order, λ is the wavelength of the X-ray source, d is the interplanar distance and Θ is the diffraction angle [68].

$$n\lambda = 2d\sin\Theta \qquad (9)$$

Diffracting planes are then matched to those of standard databases. In this work, a Bruker AXS D8 diffractometer is used equipped with $Cr-K_\alpha$ radiation source. The generator was set at 35 kV acceleration voltage and 40 mA current.

4.4 Microstructural investigation

A stereomicroscope and a scanning electron microscope are used to evaluate microstructure and fractured tensile specimen. The stereoscopic microscope is a type of optical microscope intended for low magnification observation, with light reflected from the surface of an object rather than transmitted through it. For stereomicroscopic imaging, a Zeiss discovery V20 is used together with AxioVision image analysis software. The SEM makes use of a focused electron beam. Electrons are generated either via field emission gun, tungsten source or LaB_6 source; accelerated through apertures at a rather high potential (keV). The beam is then focused by means of various electromagnetic lenses; scanning coils are used to move the electron beam over the sample surface [69]. Incoming electrons interact with the sample, resulting in energy loss of different amount. The electrons emitted from the sample surface are detected as a signal, later amplified and displayed on a TV-screen. SEM has advantages over optical microscopy in a way that depth of field is much superior, and the spatial resolution is also much better. By choosing an appropriate detector such as a backscattered electron detector, one can perform imaging using atomic number contrast. The microstructure of our RHEA as-cast sample is studied on polished and chemically etched specimen using a LEO Gemini 1550 SEM. The etchant used to reveal the microstructure is a mixture of 1.5 ml nitric acid, 5 ml Hydrofluoric acid and 45 ml water which was applied for approximately 10 seconds.

4.5 Tensile testing

Parameters such as ultimate tensile stress (the maximum stress- that a material can withstand before breaking), the maximum elongation, reduction in area, Young's modulus, yield strength and strain-hardening characteristics can be determined through material testing under tensile loading. Rectangular dog-bone-shaped tensile specimen with a gauge length of 12.5 mm, width of 3.2 mm and thickness of 2 mm, were machined from the as-cast ingot by electrical discharge machining. Tensile testing was carried out using an Instron 5500R electro-mechanic tensile tester, with a strain rate of 10^{-3} s^{-1}.

5 Results and discussions

5.1 Md concept and HEAs

Figure 9 shows the utilization of the parameter *Md* to fcc HEAs comprising of 3d transition metals as mentioned earlier in Table 3. Interestingly, there exists a clearly defined critical *Md* value, *~0.97*, below which only fcc solid solutions form, and above which TCP/GCP phases such as the σ phase, Laves phase, R phase and η phase will appear. This result is certainly appealing, as it shows the opportunity of using a single and simple parameter to anticipate the solid solubility limit in fcc HEAs, which are one of the most investigated HEAs. The critical *Md* for the sigma phase formation in Ni-based superalloys is *0.915*. For other TCP phases such as μ phase in Co-based alloys and σ phase in Fe-based alloys, the critical *Md* is reported to be *0.90* [35]. The larger critical *Md* (0.97) in HEAs, compared to those in conventional alloys, can be assumed by the increased solid solubility in HEAs and the larger compositional average.
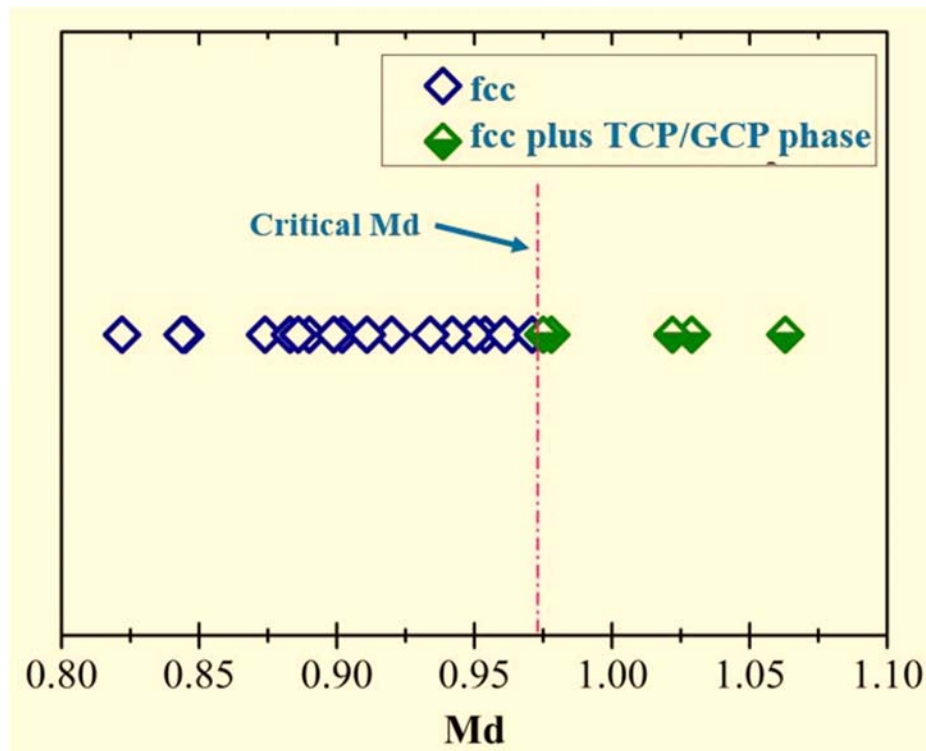

Figure 9: Md and their phase formation in fcc structured HEAs with 3d transition metals

To further complement the *Md* concept, we have reported XRD diffraction pattern for $CoCrFeNiSi_x$ (where x=0.05, 0.1, 0.15, 0.25) in Figure 10, with the aim to determine the effect of Si content on the phase stability of CoCrFeNi which is a well-studied fcc HEA (68). It appears that the currently investigated series is comprised of a single fcc structure and is in accordance to the critical solid solubility limit with *Md* value less than *0.97*. The *Md values* for $CoCrFeNiSi_{0.05}$, $CoCrFeNiSi_{0.1}$, $CoCrFeNiSi_{0.15}$ and $CoCrFeNiSi_{0.25}$ are 0.886, 0.899, 0.911 and 0.934 respectively, which are all within the critical *Md* limit.
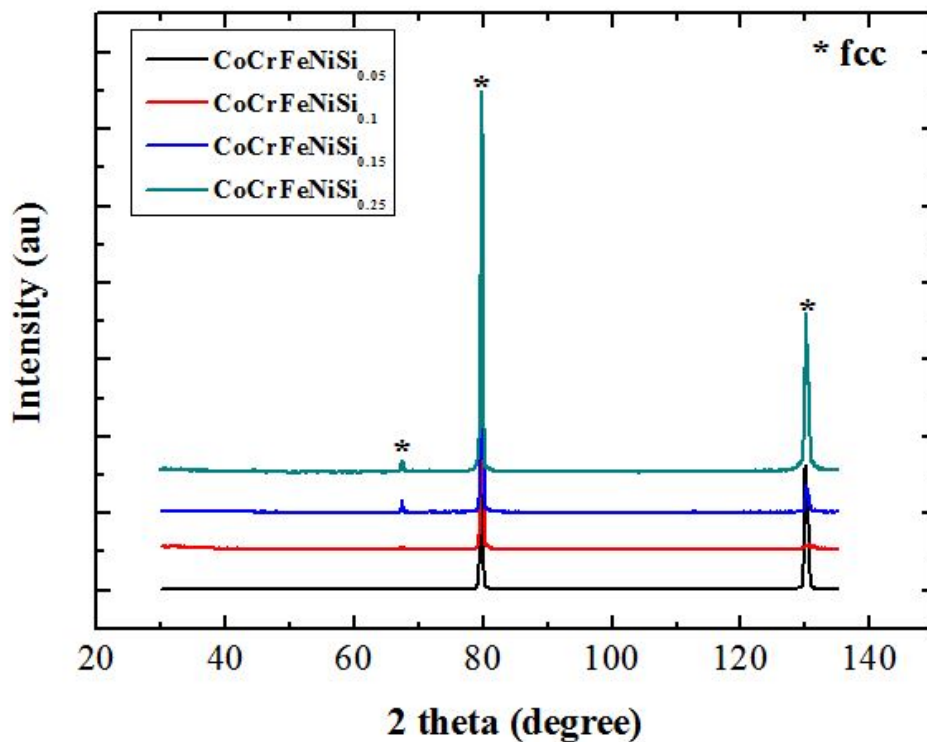
Figure 10: X-ray diffraction for CoCrFeNiSi_x (where x=0.05; 0.1; 0.15 and 0.25)

Figure 11 shows both optical micrographs and SEM images of the as-cast alloys $CoCrFeNiSi_{0.05}$ and $CoCrFeNiSi_{0.15}$ respectively. These samples are etched using A2 electrolyte (Struers) by electrolytic polishing method. Both of the as-cast alloys show a typical dendritic morphology. The HEAs appear to be without any presence of secondary phases/ intermetallics.
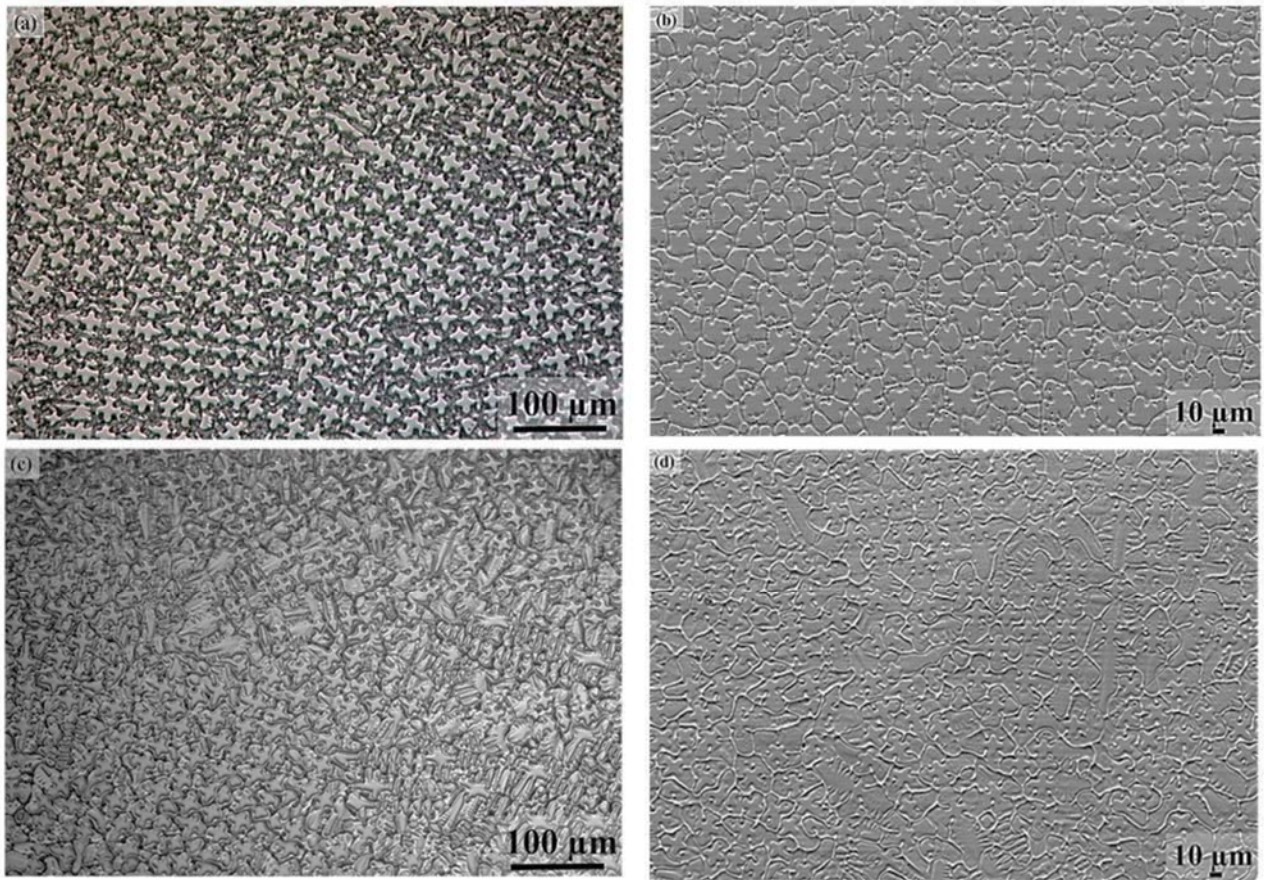
Figure 11: Images for as-cast microstructure; (a), (b) for CoCrFeNiSi$_{0.05}$ and (c), (d) for CoCrFeNiSi$_{0.15}$ under optical microscope and SEM respectively with a typical dendritic morphology

Md concept becomes more complex when 4d transition metals are alloyed. Similarly, to utilize the *Md* concept for bcc structured alloys, another parameter has to be considered, which is known as bond order, *Bo [36]*. Morinaga et al. has reported the solid solubility in bcc Fe with the conclusions that *Bo* has to be taken into consideration and *Md* alone is not enough [70]. Just like *Md*, *Bo* can also be obtained from the cluster calculation and is a measure of the strength of the covalent bond between atoms. It also varies as per the position of elements in the periodic table. *Bo* in bcc alloys is relevant to the significant second-nearest-neighbour interaction, and shorter second-nearest-neighbour interatomic distance, which is believed to be 15% larger than the first-nearest-neighbour distance. While in fcc alloys, this distance is 41% larger and hence the second-nearest-neighbour interactions is less significant, so utilizing *Bo* is not required for fcc alloys. These scenarios are discussed in detail in the attached manuscript.

28

5.2 VEC and RHEAs

Figure 12 shows the backscattered electron micrograph obtained in SEM of the as-cast alloy with dendritic structure. Regardless of heavy alloying, XRD pattern indicates a single-phase body centered cubic (bcc) structure, with all three main peaks identified. Constituent elements have bcc crystal lattices just below their melting temperatures. Binary alloying of Nb with Ta results in a bcc structure with a continuous solid solution in the entire composition range [71]. Hf, Zr and Ti also form continuous solid solutions with each other, but hexagonal close packed (hcp) crystal structure is also reported at lower temperatures due to polymorphic transformations. For the $Hf_{0.5}Nb_{0.5}Ta_{0.5}Ti_{1.5}Zr$ alloy, the formation of hcp phase is kinetically restricted and only bcc phase is formed which can be referred to the high configurational entropy and slow diffusivity of elements in the multicomponent alloys [4, 72].
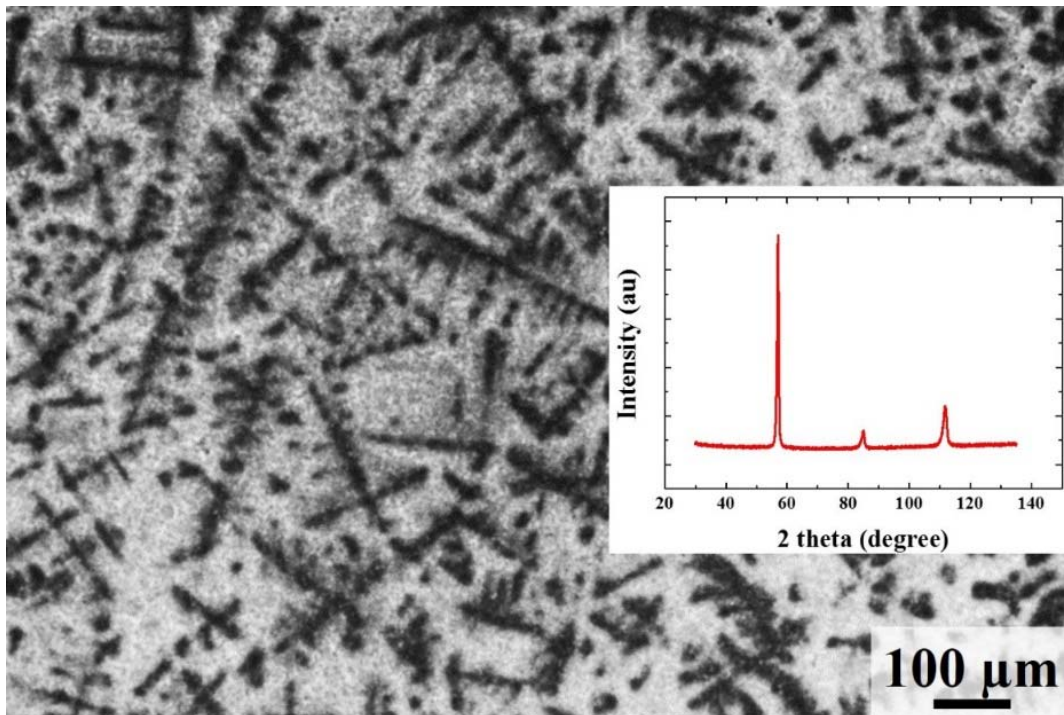

Figure 12: As-cast microstructure with a typical dendritic and inter-dendritic morphology; the alloy is of single bcc phase, as shown from the XRD inset.

It is necessary to point out that single phase solid solution is a pre-condition to justify the *VEC* concept for ductilizing RHEA in order to avoid any influence from the secondary phases. Table 7 lists nine different RHEAs containing elements from group IV, V and VI and their corresponding *VEC* values. We have tried to cover a range of alloys based on their *VEC,* with the minimum value of 4.25 and the maximum of 5.5. Among them, three are ductile RHEAs (tensile elongation > 5%) while six are brittle. These are all reported to be single phase bcc alloys.

Table 7: Refractory HEAs and their corresponding VEC.

Alloy system	VEC	Reference
HfNbTiZr	4.25	[56]
$Hf_{0.5}Nb_{0.5}Ta_{0.5}Ti_{1.5}Zr$	4.25	[This work]
HfNbTaTiZr	4.4	[23]
HfMoTaTiZr	4.6	[73]
HfMoNbTaTiZr	4.67	[73]
HfMoNbTiZr	4.6	[74]
MoNbTaVW	5.4	[8, 12]
MoNbTaW	5.5	[8, 12]
MoNbTaV	5.25	[75]

A new RHEA of type, $Hf_{0.5}Nb_{0.5}Ta_{0.5}Ti_{1.5}Zr$, has been designed, based on our intention to develop intrinsically ductile RHEAs following the electron theory, i.e. to keep *VEC* low. Ductile RHEAs have a VEC ≤ 4.4, while all brittle alloys have a VEC ≥ 4.6. With the related information of nine alloys, it is perhaps not convincing enough to conclude that there exists a threshold VEC of ~ 4.5 below which intrinsic ductility can be achieved in RHEAs. However, decreasing VEC in RHEAs by controlled alloying has indeed proven effective in ductilizing RHEAs which is further illustrated in Figure 13.
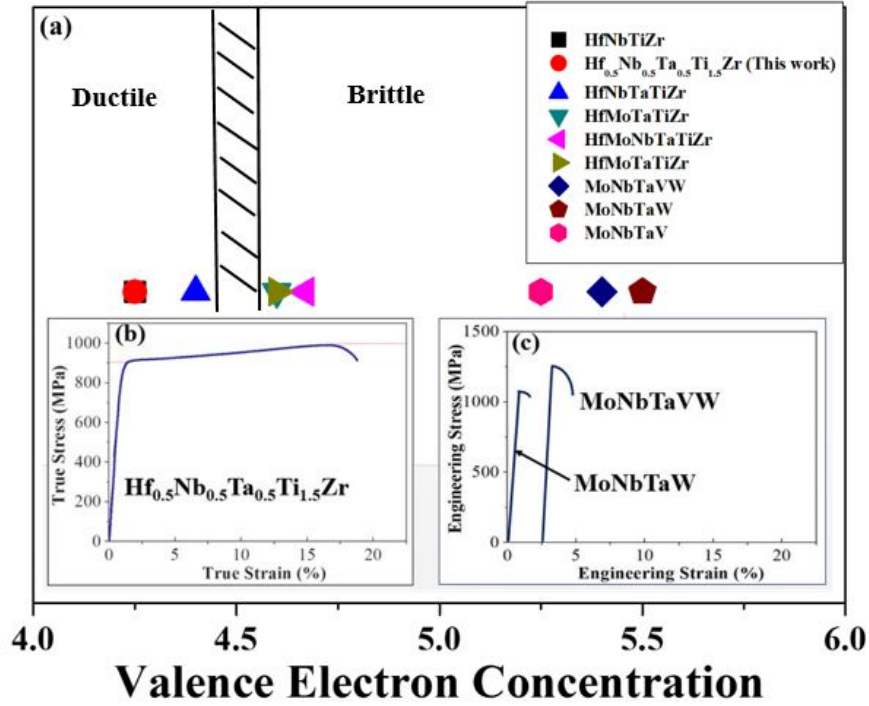
Figure 13: Plot of VEC for different RHEAs (a); Three of the alloys with lower VEC are ductile among which, two are reported and one is from this work also complemented by tensile stress-strain graph for $Hf_{0.5}Nb_{0.5}Ta_{0.5}Ti_{1.5}Zr$ (b); Alloys with higher VEC are reportedly brittle alloys and is shown by engineering stress-strain compression curves of MoNbTaVW and MoNbTaW alloys (c) [8, 12].

Interestingly, there exists a clearly shift in the material behavior based upon *VEC,* i.e. RHEAs with lower *VEC* show a combination of high fracture strength and high ductility, as shown in the tensile test result in Figure 13 (b), while at higher *VEC* the materials are brittle, as shown in the compression testing result in Figure 13 (c) [8, 12]. Alloying additions can alter the Fermi level, and therefore tune the corresponding intrinsic failure mode and critical strain for the shear instability. Lowering the number of valence electrons shifts the Fermi level down relative to the band structure, so less strain is required and the shear instability occurs much earlier. Based upon the results, it is suggested that intrinsically ductile RHEAs can be designed by controlling VEC through alloying. It has to be emphasized that the strategy is essentially directed to bcc solid solutions. The as-cast $Hf_{0.5}Nb_{0.5}Ta_{0.5}Ti_{1.5}Zr$ alloy has a room temperature tensile strength of 990 MPa and an elongation of 18.8%, in the true stress/strain condition. High fracture strength of this RHEA is referred to the strong bonding obtained from the refractory elements. Also, plastic strain to such extent is not usually found among bcc HEAs. The proof stress (determined by shifting the linear elastic curve to 0.2% strain) is determined to be 903 MPa, and the Vickers hardness is found to be 301 HV. It is

31

important to comment here that the mechanical properties of the as-cast RHEA can be further modified by thermo-mechanical treatments which will make these alloys even more attractive. The top-view of the fractured tensile specimen as observed by stereomicroscope is shown in Figure 14 (a) and, indicates deformation and necking-like behaviour. It is known that most of the common structural alloys fail through microvoid coalescence, where excessive load leads to fracture. The formation of microvoids is associated with dislocation pile-ups, grain boundaries, inclusions or due to secondary particles/phases, leading to dimple rupture for the case of ductile materials. In our case, since we are dealing with single phase alloy, microvoid formation due to secondary particles will be ruled out. It is also known that the direction of maximum stress applied has an influence on the shape of dimples formed. Under tensile testing, equiaxed and elongated dimples pointing towards fracture origin can be formed. This seems to be the case in the fracture morphology for $Hf_{0.5}Nb_{0.5}Ta_{0.5}Ti_{1.5}Zr$ alloy, as shown in Figure 14 (b), i.e. both equiaxed and elongated dimples are present. Large and smaller dimples are visible, but they seem to be rather shallow as shown in Figure 14 (c).
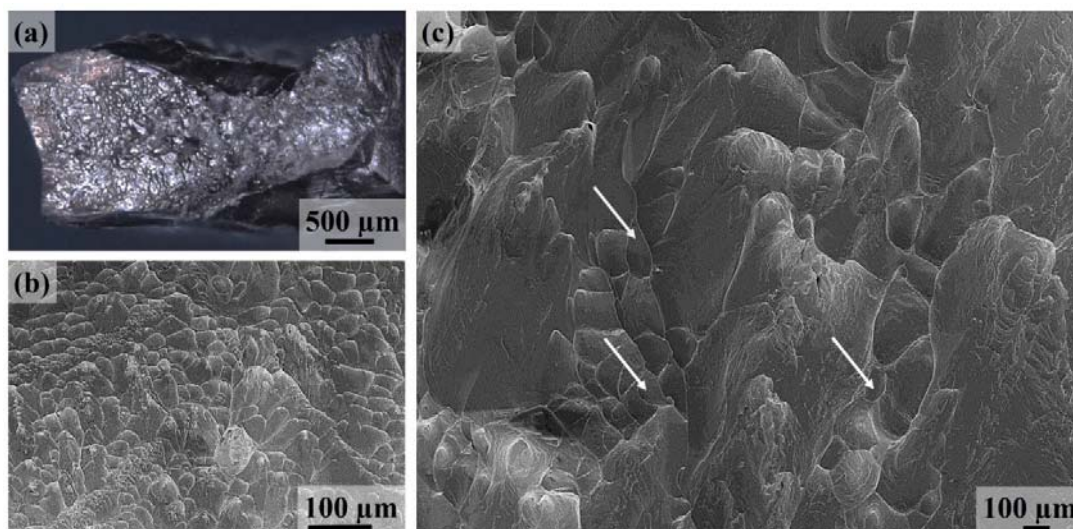

Figure 14: Fractured surface of tensile specimen $Hf_{0.5}Nb_{0.5}Ta_{0.5}Ti_{1.5}Zr$ (a) Stereomicroscopic image of the fracture surfaces with signs of necking like behaviour; (b) SEM image with both equiaxed and elongated dimples in different regions; (c) SEM image at higher magnification image showing cup shaped dimples marked by arrows.

It is significant to note here that the density of RHEA $Hf_{0.5}Nb_{0.5}Ta_{0.5}Ti_{1.5}Zr$ was measured to be 8.13 g/cm^3 using the Archimedes' principle, and is comparable to the density of current Ni-based

superalloys and lower than other RHEAs. The usual perception of most of the RHEAs is their rather high densities, such as MoNbTaVW (12.36 g/cm^3) and MoNbTaW (13.8 g/cm^3), HfNbTaTiZr (9.94 g/cm^3), HfMoTaTiZr (10.24 g/cm^3) and HfMoNbTaTiZr (9.97 g/cm^3). Based upon the estimated melting point of 2055 ^{o}C by rule of mixture, Hf$_{0.5}$Nb$_{0.5}$Ta$_{0.5}$Ti$_{1.5}$Zr certainly has potential to compete with current superalloys. Further optimization of both room and elevated temperature properties while keeping the density relatively lower, will certainly enable RHEAs to become competitive high-temperature alloys to superalloys.

Thermomechanical treatments can also be used to further improve the mechanical performance of as-cast material. A comparison of yield strength versus density of RHEA and of major material classes is given in Figure 15 [76]. There are materials which have high yield strength than current RHEA, but still, one should not forget that Hf$_{0.5}$Nb$_{0.5}$Ta$_{0.5}$Ti$_{1.5}$Zr is a single phase material with as good strength/density values as most of the current materials, and in some cases they even surpass them. Immobile structures may utilize high density materials, but aerospace industry has a constant demand for low-density metallic alloys in high-temperature thermal protection systems, especially load-bearing structures. Therefore, we have a clear motivation for exploring HEAs composed of constituents that can result in alloys with optimal mechanical properties, high melting temperatures and densities reduced as much as possible.
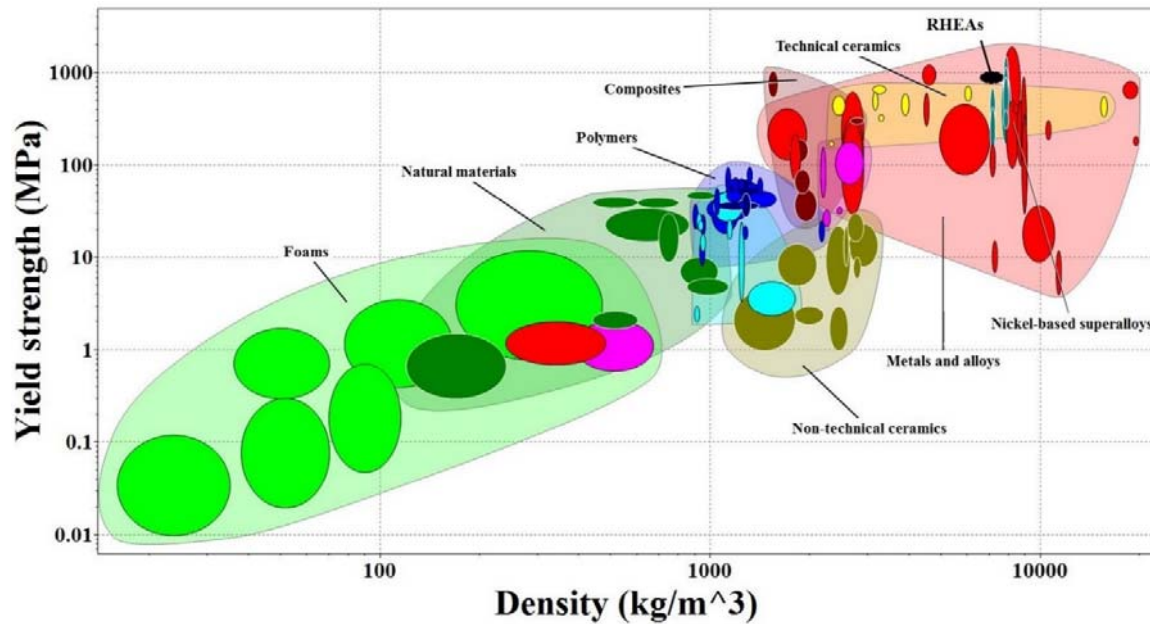
Figure 15: Ashby map showing yield strength as a function of density for Hf$_{0.5}$Nb$_{0.5}$Ta$_{0.5}$Ti$_{1.5}$Zr in relation to the wide range of material systems. The high yield strength combined with rather low density makes RHEAs potential materials for future applications.

To conclude, we have employed *VEC* to design a new ductile RHEA, Hf$_{0.5}$Nb$_{0.5}$Ta$_{0.5}$Ti$_{1.5}$Zr, with a yield stress of 903 MPa, a fracture stress of 990 MPa, a density of 8.13 g/cm^3 and an elongation of 18.8%. This material has superior properties compared to previously developed ductile RHEAs. It is proposed that lowering the *VEC*, which can be controlled by adjusting the alloy composition, seems to be a valid strategy for ductiling single phase bcc RHEAs comprising of elements from group IV, V and VI elements. This approach has so far been validated by three ductile materials with lower *VEC*: HfNbTiZr, Hf$_{0.5}$Nb$_{0.5}$Ta$_{0.5}$Ti$_{1.5}$Zr and HfNbTaTiZr, and six brittle materials with rather higher *VEC*: HfMoNbTiZr, HfMoNbTaTiZr, MoNbTaVW, MoNbTaW, MoNbTaV and HfMoTaTiZr. This outcome of alloy design using *VEC* is certainly exciting, as it opens up the prospects of using a simple and single parameter to design ductile RHEAs, which have been studied quite extensively recently.

6 Conclusions

Know-how of the phase selection in high-entropy alloys (HEAs), or multicomponent alloys with equiatomic or close-to-equiatomic compositions is of critical importance for the alloy design in this new class of advanced metallic materials, as it significantly affects their mechanical properties. Predicting the phase selection in HEAs has been relying on the parametric approach utilizing parameters that can reflect the geometrical, physiochemical and even thermodynamic properties of constituent elements or pairs of constituent elements. The parametric approach has achieved much success in predicting the formation of solid solutions, intermetallic compounds and amorphous phase in HEAs, but the lack of distinctive boundaries in forming these different phases has always been an issue. The average energy of d-orbital levels, *Md*, to predict the formation of single-phase solid solution in HEAs is proposed in this work. It is found that *Md* alone can satisfactorily delineate the formation of single phase fcc solid solution in HEAs containing 3d elements, and also in bcc structured HEAs. Our finding will greatly simplify the design of HEAs with optimal mechanical properties that are currently much relying on the solid solutions. The situation becomes more complicated when using *Md* to predict the formation of single-phase solid solution in fcc structured HEAs containing 4d elements, and also in bcc structured HEAs. The reasons that account for the complication are discussed, mainly from the electronic structure perspective.

Development of new high-temperature materials, incorporating alloys based on metals with higher operating temperatures and melting points along with optimum properties, has always been motivated for their applications, typically in aerospace and marine industries. In this regard, a new ductile RHEA with composition $Hf_{0.5}Nb_{0.5}Ta_{0.5}Ti_{1.5}Zr$ is developed. It appears to perform better than previously developed ductile RHEAs, with a density of 8.13 g/cm^3 and a yield stress of 903 MPa, a fracture stress of 990 MPa and an elongation of 18.8%. Particularly, a guideline for ductilizing RHEAs comprising group IV (Ti, Zr, Hf), V (V, Nb, Ta) and VI (Cr, Mo, W) refractory elements, using the electron theory is suggested. It is found that intrinsically ductile RHEAs can be developed by alloying elements from group VI or group V, with elements from group V or group IV; which is similar to decreasing the number of valence electrons (s + d electrons), in single-phase bcc solid solutions. Our findings will shed light on the design of refractory HEAs with optimal mechanical properties.

7 Future work

In the future studies, we have planned to extend the *Md* work to fcc structured HEAs containing 3d transition metals (Ti, V, Cr, Mn, Fe, Co, Ni, Cu). The validity of the M*d* parameter will be confirmed by testing new alloy compositions. We are well aware of the challenges in the molecular orbital approach, which certainly demands further improvement, in predicting the solid solubility limit when alloying 4d and 5d elements in fcc structured HEAs, and possibly also in bcc structured HEAs.

Some of the as-cast RHEAs presented in this work do possess an attractive combination of high strength and high ductility, but thermomechanical treatments will certainly be used to further improve the mechanical performance. Literature reporting the grain growth kinetics and grain refining effect on the RHEAs is very limited. To gain further insight into such aspects is highly critical when it comes to controlling grain structure and mechanical properties from applications perspective. We are focusing on studying the grain size dependence of RHEA through thermomechanical treatments, and its effect on the mechanical properties.

8 Acknowledgements

References

1. Perepezko, J.H., *The hotter the engine, the better.* Science, 2009. **326**(5956): p. 1068-1069.
2. Fleischer, R.L., *High-temperature, high-strength materials- An overview.* Journal of Metals, 1985. **37**(12): p. 16-20.
3. Buckman Jr, R., *Alloying of refractory metals.* ASM International, Alloying, 1988: p. 419-445.
4. Yeh, J.W., et al., *Nanostructured high-entropy alloys with multiple principal elements: Novel alloy design concepts and outcomes.* Advanced Engineering Materials, 2004. **6**(5): p. 299-303.
5. Cantor, B., et al., *Microstructural development in equiatomic multicomponent alloys.* Materials Science and Engineering A, 2004. **375-377**: p. 213-218.
6. Gali, A. and E.P. George, *Tensile properties of high- and medium-entropy alloys.* Intermetallics, 2013. **39**(0): p. 74-78.
7. Liu, W.H., et al., *Grain growth and the Hall-Petch relationship in a high-entropy FeCrNiCoMn alloy.* Scripta Materialia, 2013. **68**(7): p. 526-529.
8. Senkov, O.N., et al., *Microstructure and room temperature properties of a high-entropy TaNbHfZrTi alloy.* Journal of Alloys and Compounds, 2011. **509**(20): p. 6043-6048.
9. Senkov, O.N., et al., *Mechanical properties of low-density, refractory multi-principal element alloys of the Cr-Nb-Ti-V-Zr system.* Materials Science and Engineering a-Structural Materials Properties Microstructure and Processing, 2013. **565**: p. 51-62.
10. Senkov, O.N., et al., *Low-density, refractory multi-principal element alloys of the Cr-Nb-Ti-V-Zr system: Microstructure and phase analysis.* Acta Materialia, 2013. **61**(5): p. 1545-1557.
11. Senkov, O.N., et al., *Refractory high-entropy alloys.* Intermetallics, 2010. **18**(9): p. 1758-1765.
12. Senkov, O.N., et al., *Mechanical properties of $Nb_{25}Mo_{25}Ta_{25}W_{25}$ and $V_{20}Nb_{20}Mo_{20}Ta_{20}W_{20}$ refractory high entropy alloys.* Intermetallics, 2011. **19**(5): p. 698-706.
13. Senkov, O.N. and C.F. Woodward, *Microstructure and properties of a refractory NbCrMo0.5Ta0.5TiZr alloy.* Materials Science and Engineering a-Structural Materials Properties Microstructure and Processing, 2011. **529**: p. 311-320.
14. Yeh, J.W., *Recent progress in high-entropy alloys.* Annales De Chimie-Science Des Materiaux, 2006. **31**(6): p. 633-648.
15. Wu, W.H., C.C. Yang, and J.W. Yeh, *Industrial development of high-entropy alloys.* Annales De Chimie-Science Des Materiaux, 2006. **31**(6): p. 737-747.
16. Porter, D.A., K.E. Easterling, and M. Sherif, *Phase Transformations in Metals and Alloys, (Revised Reprint).* 2009: CRC press.
17. Swalin, R.A., *Thermodynamics of Solids, 2nd Ed.* 1991, New York: Wiley.
18. Gaskell, D.R., *Introduction to the Thermodynamics of Materials.* 2008: CRC Press.
19. Yeh, J.W., *Alloy Design Strategies and Future Trends in High-Entropy Alloys.* Jom, 2013. **65**(12): p. 1759-1771.
20. Gao, M.C., et al., *High-Entropy Alloys: Fundamentals and Applications.* 2016, Cham, Switzerland: Springer.
21. Otto, F., et al., *Relative effects of enthalpy and entropy on the phase stability of equiatomic high-entropy alloys.* Acta Materialia, 2013. **61**(7): p. 2628-2638.

22. Tsai, K.Y., M.H. Tsai, and J.W. Yeh, *Sluggish diffusion in Co-Cr-Fe-Mn-Ni high-entropy alloys.* Acta Materialia, 2013. **61**(13): p. 4887-4897.

23. Dirras, G., et al., *Elastic and plastic properties of as-cast equimolar TiHfZrTaNb high-entropy alloy.* Materials Science and Engineering A, 2016. **654**: p. 30-38.

24. Yeh, J.W., et al., *Anomalous decrease in X-ray diffraction intensities of Cu-Ni-Al-Co-Cr-Fe-Si alloy systems with multi-principal elements.* Materials Chemistry and Physics, 2007. **103**(1): p. 41-46.

25. Zhang, Y., et al., *Minor alloying behavior in bulk metallic glasses and high-entropy alloys.* Science in China Series G-Physics Mechanics & Astronomy, 2008. **51**(4): p. 427-437.

26. Kaviany, M., *Heat Transfer Physics.* 2014: Cambridge University Press.

27. Swalin, R., *Thermodynamics of Solids.* Wiley-Interscience, New York. 1972.

28. Ranganathan, S., *Alloyed pleasures: Multimetallic cocktails.* Current Science, 2003. **85**(10): p. 1404-1406.

29. Guo, S. and C.T. Liu, *Phase stability in high entropy alloys: Formation of solid-solution phase or amorphous phase.* Progress in Natural Science: Materials International, 2011. **21**(6): p. 433-446.

30. Zhang, Y., et al., *Solid-solution phase formation rules for multi-component alloys.* Advanced Engineering Materials, 2008. **10**(6): p. 534-538.

31. Zhang, Y., X. Yang, and P.K. Liaw, *Alloy design and properties optimization of high-entropy alloys.* JOM, 2012. **64**(7): p. 830-838.

32. Yang, X. and Y. Zhang, *Prediction of high-entropy stabilized solid-solution in multi-component alloys.* Materials Chemistry and Physics, 2012. **132**(2-3): p. 233-238.

33. Guo, S., et al., *Effect of valence electron concentration on stability of fcc or bcc phase in high entropy alloys.* Journal of Applied Physics, 2011. **109**(10): p. 103505.

34. Guo, S., et al., *More than entropy in high-entropy alloys: Forming solid solutions or amorphous phase.* Intermetallics, 2013. **41**: p. 96-103.

35. Morinaga, M., et al., *Solid solubilities in transition-metal-based fcc alloys.* Philosophical Magazine A, 1985. **51**(2): p. 223-246.

36. Adachi, H., T. Mukoyama, and J. Kawai, *Hartree–Fock–Slater Method for Materials Science: The DV-Xα Method for Design and Characterization of Materials.* 2005, Berlin: Springer. 23-48.

37. Morinaga, M., et al., *New PHACOMP and its application to alloy design.* Superalloys 1984, 1984: p. 523-532.

38. Bozzolo, G., R.D. Noebe, and P.B. Abel, *Applied Computational Materials Modeling: Theory, Simulation and Experiment.* 2007: Springer Science & Business Media.

39. Tong, C.J., et al., *Microstructure characterization of Al_xCoCrCuFeNi high-entropy alloy system with multiprincipal elements.* Metallurgical and Materials Transactions A, 2005. **36**(4): p. 881-893.

40. Hsu, Y.J., W.C. Chiang, and J.W. Wu, *Corrosion behavior of FeCoNiCrCu_x high-entropy alloys in 3.5% sodium chloride solution.* Materials Chemistry and Physics, 2005. **92**(1): p. 112-117.

41. Lucas, M.S., et al., *Absence of long-range chemical ordering in equimolar FeCoCrNi.* Applied Physics Letters, 2012. **100**(25): p. 251907.

42. Wang, X.F., et al., *Novel microstructure and properties of multicomponent CoCrCuFeNiTi_x alloys.* Intermetallics, 2007. **15**(3): p. 357-362.

43. Zhang, Y., G.L. Chen, and L. Gan, *Phase change and mechanical behaviors of $Ti_xCoCrFeNiCu_{1-y}Al_y$ high entropy alloys.* Journal of ASTM International, 2010. **7**(5): p. Paper ID: JAI102527

44. Kao, Y.F., et al., *Microstructure and mechanical property of as-cast, -homogenized, and -deformed $Al_xCoCrFeNi$ (0 <= x <= 2) high-entropy alloys.* Journal of Alloys and Compounds, 2009. **488**(1): p. 57-64.

45. Chen, M.R., et al., *Effect of vanadium addition on the microstructure, hardness, and wear resistance of $Al_{0.5}CoCrCuFeNi$ high-entropy alloy.* Metallurgical and Materials Transactions A, 2006. **37**(5): p. 1363-1369.

46. Shun, T.T., L.Y. Chang, and M.H. Shiu, *Microstructures and mechanical properties of multiprincipal component $CoCrFeNiTi_x$ alloys.* Materials Science and Engineering A, 2012. **556**: p. 170-174.

47. Sheikh, S. and S. Guo, Unpublished results.

48. Chuang, M.H., et al., *Microstructure and wear behavior of $Al_xCo_{1.5}CrFeNi_{1.5}Ti_y$ high-entropy alloys.* Acta Materialia, 2011. **59**(16): p. 6308-6317.

49. Shun, T.T., C.H. Hung, and C.F. Lee, *The effects of secondary elemental Mo or Ti addition in $Al_{0.3}CoCrFeNi$ high-entropy alloy on age hardening at 700 ºC.* Journal of Alloys and Compounds, 2010. **495**(1): p. 55-58.

50. Chen, H.Y., et al., *Effect of the substitution of Co by Mn in Al-Cr-Cu-Fe-Co-Ni high-entropy alloys.* Annales De Chimie-Science Des Materiaux, 2006. **31**(6): p. 685-698.

51. Chen, M.R., et al., *Microstructure and properties of $Al_{0.5}CoCrCuFeNiTi_x$ (x=0-2.0) high-entropy alloys.* Materials Transactions, 2006. **47**(5): p. 1395-1401.

52. Ma, S.G. and Y. Zhang, *Effect of Nb addition on the microstructure and properties of AlCoCrFeNi high-entropy alloy.* Materials Science and Engineering A, 2012. **532**: p. 480-486.

53. *www.vertex42.com/Files/pdfs/2/periodic-table.pdf*.

54. *www.haynesintl.com/230HaynesAlloy.htm*.

55. *www.specialmetals.com/inconel-alloy-718*.

56. Wu, Y.D., et al., *A refractory $Hf_{25}Nb_{25}Ti_{25}Zr_{25}$ high-entropy alloy with excellent structural stability and tensile properties.* Materials Letters, 2014. **130**: p. 277-280.

57. Liu, G., et al., *Nanostructured high-strength molybdenum alloys with unprecedented tensile ductility.* Nature materials, 2013. **12**(4): p. 344-350.

58. Kelly, A., W. Tyson, and A. Cottrell, *Ductile and brittle crystals.* Philosophical magazine, 1967. **15**(135): p. 567-586.

59. Rice, J.R. and R. Thomson, *Ductile versus brittle behaviour of crystals.* Philosophical magazine, 1974. **29**(1): p. 73-97.

60. Chan, K.S., *A computational approach to designing ductile Nb-Ti-Cr-Al solid-solution alloys.* Metallurgical and Materials Transactions A, 2001. **32**(10): p. 2475-2487.

61. Peierls, R., *The size of a dislocation.* Proceedings of the Physical Society, 1940. **52**(1): p. 34.

62. Nabarro, F., *Dislocations in a simple cubic lattice.* Proceedings of the Physical Society, 1947. **59**(2): p. 256.

63. Qi, L. and D.C. Chrzan, *Tuning ideal tensile strengths and intrinsic ductility of bcc refractory alloys.* Physical Review Letters, 2014. **112**(11): p. 115503.

64. Li, X., et al., *Ab initio-predicted micro-mechanical performance of refractory high-entropy alloys.* Scientific reports, 2015. **5**: p. 12334.

65. Liu, C.T. and J.O. Stiegler, *Ductile ordered intermetallic alloys*. Science, 1984. **226**(4675): p. 636-642.

66. Mizutani, U., *Hume-Rothery Rules for Structurally Complex Alloy Phases*. 2011, Boca Raton: CRC Press.

67. Massalski, T.B., *Comments concerning some features of phase diagrams and phase transformations*. Materials Transactions, 2010. **51**(4): p. 583-596.

68. Kelly, A., G.W. Groves, and P. Kidd, *Crystallography and Crystal Defects*. 2000: John Wiley & Sons.

69. Goldstein, J., *Practical Scanning Electron Microscopy: Electron and Ion Microprobe Analysis*. 2012: Springer Science & Business Media.

70. Morinaga, M., N. Yukawa, and H. Adachi, *Alloying effect on the electronic structure of BCC Fe*. Journal of Physics F: Metal Physics, 1985. **15**(5): p. 1071.

71. Massalski, T.B., et al., *Binary Alloy Phase Diagrams. vol. 3*. ASM International, 1990, 1990.

72. Yeh, J.W., et al., *High-entropy alloys - A new era of exploitation*. Materials Science Forum, 2007. **560**: p. 1-9.

73. Juan, C.C., et al., *Enhanced mechanical properties of HfMoTaTiZr and HfMoNbTaTiZr refractory high-entropy alloys*. Intermetallics, 2015. **62**: p. 76-83.

74. Guo, N.N., et al., *Microstructure and mechanical properties of refractory MoNbHfZrTi high-entropy alloy*. Materials & Design, 2015. **81**: p. 87-94.

75. Yao, H.W., et al., *MoNbTaV medium-entropy alloy*. Entropy, 2016. **18**(5): p. doi:10.3390/e18050189.

76. Ashby, M.F., *Materials Selection in Mechanical Design, Fourth Edition*. 2011, Amsterdam: Elsevier.